

Numerical strategies for variational updates in large strain inelasticity with incompressibility constraint

Marian Sielenkämper¹ | Jan Dittmann¹ | Stephan Wulfinghoff

Computational Materials Science,
Institute for Materials Science, Kiel
University, Kiel, Germany

Correspondence

Marian Sielenkämper, Computational
Materials Science, Institute for Materials
Science, Kiel University, Kaiserstr. 2,
24143 Kiel, Germany.
Email: mfs@tf.uni-kiel.de

Funding information

German Research Foundation,
Grant/Award Numbers: WU847/3-1, GRK
2154/1

Abstract

In finite deformation inelasticity, one often has to deal with the incompressibility constraint. In the past, this was dealt with using, for example, an exponential mapping approach, which yields exact volume preservation in plastic deformations. In this article however, the special-linear update approach by Hurtado et al. *The special-linear update: An application of differential manifold theory to the update of isochoric plasticity flow rules*, Int J Numer Methods Eng. 2014;97(4):298-312, which utilizes a projection method to fulfill the incompressibility constraint is used. The model is applied to isotropic plasticity by a novel approximation of the logarithm and treats kinematic hardening without losing the symmetry of the internal variables. The model results are compared to models utilizing an exponential mapping approach in numerical experiments.

KEYWORDS

finite deformation plasticity, incompressibility constraint, inelasticity, kinematic hardening, projection method

1 | INTRODUCTION

Nowadays, when modeling finite deformation plasticity or other inelastic deformations, the multiplicative split of the deformation gradient, that is, $\mathbf{F} = \mathbf{F}^e \mathbf{F}^p$, introduced by Eckhart,¹ Kröner,² and Lee³ is widely accepted. Using this approach, one often has to deal with the incompressibility constraint, which is motivated by the observation that plastic deformations occur due to dislocation glide. In recent time, many finite deformation plasticity algorithms use an exponential mapping approach (see, e.g., References 4-7) to cope with the incompressibility constraint. The advantage of using the exponential map approach is the intrinsic exact fulfillment of the incompressibility constraint. Moreover, the formulation is very neat and compact. However, it is not always obvious how to preserve the symmetry of the involved variables (see Dettmer and Reese⁶). Further, the exponential map comes with the disadvantage of having to perform a spectral decomposition, which is numerically elaborate. Additionally, while manageable, the linearization of the exponential map is not always straightforward (see, e.g., Ortiz et al.⁸). In this article, the special-linear update by Hurtado et al.,⁹ which is an alternative to the exponential mapping approach is used. It also exactly satisfies the incompressibility constraint. For the kinematic hardening model, there are mainly two different types found in the literature. Some models are of the Chaboche-type, which makes use of evolution equations for the update of the back stress (see, e.g., References 10,11). The other family of models makes use of a further multiplicative split of the plastic deformation gradient \mathbf{F}^p into an energetic

This is an open access article under the terms of the Creative Commons Attribution-NonCommercial-NoDerivs License, which permits use and distribution in any medium, provided the original work is properly cited, the use is non-commercial and no modifications or adaptations are made.

© 2021 The Authors. *International Journal for Numerical Methods in Engineering* published by John Wiley & Sons Ltd.

and a dissipative part (see Lion¹² and Dettmer and Reese⁶), which is an extension of the Frederick–Armstrong model.¹³ For the model presented in this article, the latter is used.

This article is structured as follows. First, the theory and numerical treatment of the model are discussed in Section 2. Here, the time-discrete counterpart for the isotropic hardening potential is given as well. In Section 3, results for the isotropic hardening model are shown. Next, the model is extended for the incorporation of kinematic hardening in Section 4, where the results for kinematic hardening are also presented. Finally, a summary and outlook is given in Section 5.

2 | MODELING OF FINITE DEFORMATION PLASTICITY

2.1 | Kinematics

The finite deformation of a body can be described by using the gradient of deformation $\mathbf{x}(\mathbf{X}, t)$

$$\mathbf{F} = \text{Grad}(\mathbf{x}), \quad (1)$$

which relates line elements of a body in the reference configuration to the current configuration. Then, one often defines

$$J = \det(\mathbf{F}), \quad (2)$$

which describes the volumetric part of the deformation. In finite deformation plasticity, one often splits \mathbf{F} multiplicatively, that is,

$$\mathbf{F} = \mathbf{F}^e \mathbf{F}^p, \quad (3)$$

where \mathbf{F}^e is the elastic part and \mathbf{F}^p is the plastic part of the deformation gradient (see Kröner² and Lee³). To incorporate kinematic hardening, the additional multiplicative split of \mathbf{F}^p , employed by Lion¹² as well as Dettmer and Reese,⁶ is introduced as

$$\mathbf{F}^p = \mathbf{F}^{pe} \mathbf{F}^{pd}, \quad \det(\mathbf{F}^p) = 1, \quad \det(\mathbf{F}^{pe}) = \det(\mathbf{F}^{pd}) = 1, \quad (4)$$

where \mathbf{F}^{pe} is the energetic and \mathbf{F}^{pd} the dissipative part of \mathbf{F}^p . Note that \mathbf{F}^{pe} as well as \mathbf{F}^{pd} have to be both unimodular. Further, one commonly introduces the elastic left Cauchy–Green tensor \mathbf{b}^e and the plastic right Cauchy–Green tensor \mathbf{C}^p as

$$\begin{aligned} \mathbf{b}^e &= \mathbf{F}^e \mathbf{F}^{eT} = \mathbf{F} \mathbf{C}^{p-1} \mathbf{F}^T, \\ \mathbf{C}^p &= \mathbf{F}^{pT} \mathbf{F}^p. \end{aligned} \quad (5)$$

Likewise, kinematic quantities for the dissipative and energetic parts are introduced as

$$\begin{aligned} \mathbf{C}^{pd} &= \mathbf{F}^{pdT} \mathbf{F}^{pd}, \\ \mathbf{b}^{pe} &= \mathbf{F}^{pe} \mathbf{F}^{peT} = \mathbf{F}^p \mathbf{C}^{pd-1} \mathbf{F}^{pT}. \end{aligned} \quad (6)$$

Moreover, one defines the plastic “velocity gradient” \mathbf{L}^p as

$$\mathbf{L}^p = \dot{\mathbf{F}}^p \mathbf{F}^{p-1}, \quad (7)$$

where $\dot{\bullet}$ denotes a derivative with respect to time. Correspondingly, one defines the symmetric part of the plastic velocity gradient:

$$\mathbf{D}^p = \text{sym}(\mathbf{L}^p) = \frac{1}{2} \mathbf{F}^{p-T} \dot{\mathbf{C}}^p \mathbf{F}^{p-1}. \quad (8)$$

2.2 | Casting finite deformation plasticity into the generalized standard materials framework

To ensure thermodynamic consistency, the model is cast into the generalized standard materials (GSM) framework, which was first introduced by Halphen and Nguyen.¹⁴ The Clausius–Duhem inequality for isothermal processes reads

$$D = \boldsymbol{\tau} : \mathbf{d} - \dot{\psi} \geq 0, \quad (9)$$

where D is the dissipation density, \mathbf{d} is the symmetric velocity gradient with respect to the current configuration and the Kirchhoff stress $\boldsymbol{\tau}$ is defined as $\boldsymbol{\tau} = \mathbf{F}\mathbf{S}\mathbf{F}^T = J\boldsymbol{\sigma}$. Here, \mathbf{S} is the second Piola–Kirchhoff stress tensor and $\boldsymbol{\sigma}$ is the Cauchy stress tensor. Additionally, ψ is the Helmholtz free energy density, which is introduced as the sum of all energy storage functions and reads for this work

$$\psi = \psi_e(\mathbf{b}^e) + \psi_h(\alpha) + \psi_k(\mathbf{b}^{pe}), \quad (10)$$

where $\psi_e(\mathbf{b}^e)$ is the elastic energy density, ψ_h the stored isotropic hardening energy density due to isotropic hardening and $\psi_k(\mathbf{b}^{pe})$ the stored hardening energy due to kinematic hardening. Further, α is an isotropic internal hardening variable. For the elastic energy density, a Neo-Hookean elastic energy, which is only dependent on \mathbf{b}^e , in the form of

$$\psi_e(\mathbf{b}^e) = \frac{\lambda}{4} (J^{e2} - 1 - 2 \ln(J^e)) + \frac{\mu}{2} (\mathbf{I}_{\mathbf{b}^e} - 3 - 2 \ln(J^e)) \quad (11)$$

is chosen. Here, λ and μ are the Lamé parameters and $\mathbf{I}_{\mathbf{b}^e}$ is the first invariant of \mathbf{b}^e . For ψ_h , different choices, depending on the material that is to be modeled, can be made. However, we assume ψ_h to be an increasing function, that is,

$$\frac{\partial \psi_h}{\partial \alpha} \geq 0. \quad (12)$$

The kinematic hardening energy is assumed to be only dependent on $\mathbf{I}_{\mathbf{b}^{pe}}$, the first invariant of \mathbf{b}^{pe} , and reads

$$\begin{aligned} \psi_k(\mathbf{b}^{pe}) &= \frac{\mu^p}{2} \mathbf{I}_{\mathbf{b}^{pe}}, \\ \mathbf{I}_{\mathbf{b}^{pe}} &= \text{tr}(\mathbf{b}^{pe}) = \mathbf{C}^p : \mathbf{C}^{pd-1}. \end{aligned} \quad (13)$$

Further, to complete the requirements for the GSM-framework, the dissipation potential $\phi(\mathbf{D}^p, \dot{\alpha})$ is defined in similar fashion to Han and Reddy¹⁵ as

$$\phi(\mathbf{D}^p, \dot{\alpha}) = \begin{cases} \sqrt{\frac{2}{3}} \sigma_{y0} \|\mathbf{D}^p\| & \text{tr}(\mathbf{D}^p) = 0 \wedge \dot{\alpha} \geq \sqrt{\frac{2}{3}} \|\mathbf{D}^p\| \\ \infty & \text{else.} \end{cases} \quad (14)$$

Here, σ_{y0} is the initial yield stress. Note that the if-else construct ensures that $\text{tr}(\mathbf{D}^p) = 0$ is always true when minimizing the potential, and therefore guarantees volume preserving plastic deformations. Additionally, it ensures that the normalization condition $\dot{\alpha} \geq \sqrt{2/3} \|\mathbf{D}^p\|$ always holds. To obtain the yield criterion as well as the evolution of the internal variables, the dual potential $\phi^*(\boldsymbol{\Sigma}, q)$ is introduced as

$$\phi^*(\boldsymbol{\Sigma}, q) = \sup_{\mathbf{D}^p, \dot{\alpha}} (\boldsymbol{\Sigma} : \mathbf{D}^p + q\dot{\alpha} - \phi(\mathbf{D}^p, \dot{\alpha})) \quad (15)$$

$$= \sup_{\substack{\mathbf{D}^p = \mathbf{D}^{p'} \\ \dot{\alpha} \geq \sqrt{\frac{2}{3}} \|\mathbf{D}^p\|}} (\boldsymbol{\Sigma} : \mathbf{D}^p + q\dot{\alpha} - \sqrt{\frac{2}{3}} \sigma_{y0} \|\mathbf{D}^p\|), \quad (16)$$

utilizing a Legendre–Fenchel transformation. Here, $\boldsymbol{\Sigma}$ and q are the dual variables to \mathbf{D}^p and $\dot{\alpha}$, respectively. For $q \leq 0$, obviously

$$\dot{\alpha} = \sqrt{\frac{2}{3}} \|\mathbf{D}^p\| \quad (17)$$

always holds. Additionally, replacing Σ by its deviator Σ' drops the constraint $D^p = D^{p'}$, as follows

$$\begin{aligned}
 \phi^*(\Sigma, q \leq 0) &= \sup_{\substack{D^p \\ \dot{\alpha} \geq \sqrt{\frac{2}{3}} \|D^p\|}} \left(\Sigma' : D^p - \sqrt{\frac{2}{3}} (\sigma_{y0} - q) \|D^p\| \right) \\
 &= \sup_{\gamma \geq 0} \sup_{\substack{N \\ \|N\|=1}} \left(\gamma \Sigma' : N - \sqrt{\frac{2}{3}} (\sigma_{y0} - q) \gamma \right) \\
 &= \sup_{\gamma \geq 0} \gamma \left(\|\Sigma'\| - \sqrt{\frac{2}{3}} (\sigma_{y0} - q) \right) \\
 &= \sup_{\gamma \geq 0} \gamma f(\Sigma, q \leq 0), \tag{18}
 \end{aligned}$$

where it was used that the supremum in N is achieved for $N \parallel \Sigma'$, that is,

$$D^p = \gamma \frac{\Sigma'}{\|\Sigma'\|}, \tag{19}$$

corresponding to the normality rule. Here, f is the yield criterion, which reads

$$f = \|\Sigma'\| - \sqrt{\frac{2}{3}} (\sigma_{y0} - q). \tag{20}$$

Now, $\phi^*(\sigma, q \leq 0)$ can be given in terms of f as

$$\phi^*(\sigma, q \leq 0) = \begin{cases} 0 & f \leq 0 \\ \infty & f > 0. \end{cases} \tag{21}$$

Further, since ϕ and ϕ^* are convex, utilizing a Legendre–Fenchel transformation again, we obtain

$$\begin{aligned}
 \phi(D^p, \dot{\alpha}) &= \sup_{\Sigma, q \leq 0} (\sigma : D^p + q \dot{\alpha} - \phi^*(\Sigma, q)) \\
 &= \sup_{\Sigma, q \leq 0} (\sigma : D^p + q \dot{\alpha} - \sup_{\Sigma, q \leq 0} \gamma f). \tag{22}
 \end{aligned}$$

For $f > 0$, the term $-\sup \gamma f$ in Equation (22) equals negative infinity. This definitely is not a solution of the first supremum problem in Equation (22). Now, utilizing these findings, the Karush–Kuhn–Tucker conditions follow as

$$\gamma \geq 0, \quad f \leq 0, \quad \gamma f = 0. \tag{23}$$

With the dissipation potential ϕ and the free energy density ψ at hand, one now can formulate the rate potential as

$$\pi = \frac{\partial \psi}{\partial \mathbf{F}} : \dot{\mathbf{F}} + \frac{\partial \psi}{\partial \mathbf{C}^p} : \dot{\mathbf{C}}^p + \frac{\partial \psi}{\partial \alpha} \dot{\alpha} + \phi(D^p, \dot{\alpha}), \tag{24}$$

where \mathbf{C}^p and $\dot{\alpha}$ are the internal variables. Here, it can easily verified that the second term of Equation (24) can be reformulated to

$$\frac{\partial \psi}{\partial \mathbf{C}^p} : \dot{\mathbf{C}}^p = \underbrace{2\mathbf{F}^p \frac{\partial \psi}{\partial \mathbf{C}^p} \mathbf{F}^{pT}}_{=:-\Sigma^{\text{eff}}} : D^p. \tag{25}$$

Minimizing the rate potential from Equation (24) in the internal variables while using the definition of Σ^{eff} , one realizes that the minimization of π naturally involves the definition of the dual dissipation potential ϕ^* :

$$\begin{aligned} \inf_{\mathbf{D}^p, \dot{\alpha}} \pi &= \frac{\partial \psi}{\partial \mathbf{F}} : \dot{\mathbf{F}} - \sup_{\mathbf{D}^p, \dot{\alpha}} \left(\Sigma^{\text{eff}} : \mathbf{D}^p - \underbrace{\frac{\partial \psi}{\partial \alpha} \dot{\alpha}}_{=: q_h \leq 0} - \phi(\mathbf{D}^p, \dot{\alpha}) \right) \\ &= \frac{\partial \psi}{\partial \mathbf{F}} : \dot{\mathbf{F}} - \phi^*(\Sigma^{\text{eff}}, q_h), \end{aligned} \quad (26)$$

where $q_h \leq 0$ follows from Equation (12) and we assumed that $f(\Sigma^{\text{eff}}, q_h) \leq 0$. From Equations (17), (19) and (26) it follows that

$$\mathbf{D}^p = \gamma \frac{\Sigma^{\text{eff}}}{\|\Sigma^{\text{eff}}\|}, \quad \dot{\alpha} = \sqrt{\frac{2}{3}} \|\mathbf{D}^p\| = \sqrt{\frac{2}{3}} \gamma. \quad (27)$$

Additionally, note that

$$\Sigma^{\text{eff}} = \Sigma^e - \Sigma^b, \quad (28)$$

with the elastic Mandel stress tensor $\Sigma^e = \mathbf{C}^e \mathbf{S}^e$. Further, the elastic second Piola-Kirchhoff stress \mathbf{S}^e and the Mandel back stress Σ^b are defined as

$$\mathbf{S}^e = 2 \frac{\partial \psi_e}{\partial \mathbf{C}^e}, \quad \Sigma^b = 2 \mathbf{b}^{\text{pe}} \frac{\partial \psi_k}{\partial \mathbf{b}^{\text{pe}}}. \quad (29)$$

With these definitions, one ends up with the yield criterion (cf. with Equations 20 and (26)):

$$f = \|(\Sigma^e - \Sigma^b)'\| - \sqrt{\frac{2}{3}} (\sigma_{y0} - q) \leq 0. \quad (30)$$

For \mathbf{D}^{pd} , the Frederick–Armstrong hardening model assumes

$$\mathbf{D}^{\text{pd}} = \gamma \frac{b}{a} \Sigma^b', \quad (31)$$

where a and b are material constants. The incorporation of kinematic hardening will be treated in Section 4.

2.3 | Time discretization of the rate potential for isotropic hardening

This section only focuses of the handling of isotropic hardening, since the incorporation of kinematic hardening into the algorithmic counterpart of π needs some additional careful treatment, and is therefore done in Section 4. To solve the problem equations numerically, the time has to be discretized into time steps. This is done in a conventional manner, which is described in Appendix A.

A possible transformation of the dissipation potential from Equation (14) into the algorithmic counterpart ϕ_Δ reads

$$\phi_\Delta(\mathbf{C}^p, \alpha) = \begin{cases} \frac{1}{2} \sqrt{\frac{2}{3}} \sigma_{y0} \|\mathbf{c}^p - \mathbf{I}\| & \det(\mathbf{c}^p) = 0; \Delta\alpha \geq \sqrt{\frac{2}{3}} \frac{1}{2} \|\mathbf{c}^p - \mathbf{I}\| \\ \infty & \text{else,} \end{cases} \quad (32)$$

where \mathbf{c}^p can be interpreted as the incremental counterpart of \mathbf{C}^p , which is defined as

$$\mathbf{c}^p = \mathbf{U}_n^{\text{p-1}} \mathbf{C}^p \mathbf{U}_n^{\text{p-1}}. \quad (33)$$

Here, \mathbf{U}^p is the right plastic stretch tensor of the polar decomposition $\mathbf{F}^p = \mathbf{R}^p \mathbf{U}^p$, that is, $\mathbf{U}^p = \sqrt{\mathbf{C}^p}$. The choice of using $1/2 \ln(\mathbf{c}^p)$ in the dissipation potential was introduced by Ortiz and Stainier¹⁶ and $(\mathbf{c}^p - \mathbf{I})/2$ may be thought of as a linear approximation of the logarithm. For a unimodular \mathbf{c}^p and $\Delta t \rightarrow 0$, the algorithmic approximation becomes

$$\begin{aligned} \lim_{\Delta t \rightarrow 0} \frac{1}{\Delta t} \phi_\Delta &= \sqrt{\frac{2}{3}} \sigma_{y0} \left\| \frac{1}{2} \mathbf{U}^{p-1} \dot{\mathbf{C}}^p \mathbf{U}^{p-1} \right\| \\ &= \sqrt{\frac{2}{3}} \sigma_{y0} \left\| \frac{1}{2} \mathbf{F}^{p-T} \dot{\mathbf{C}}^p \mathbf{F}^{p-1} \right\| \\ &= \sqrt{\frac{2}{3}} \sigma_{y0} \|\mathbf{D}^p\|, \end{aligned} \quad (34)$$

which is obviously in line with Equations (A1) and (14). Now, having obtained a consistent approximation for ϕ , one defines the algorithmic approximation π_Δ of π (cf. Equation (24)), which reads

$$\pi_\Delta = \psi - \psi_n + \phi_\Delta. \quad (35)$$

Further, the updates of internal variables may be obtained by solving the minimization problem

$$\inf_{\substack{\mathbf{C}^p, \alpha \\ \det(\mathbf{C}^p)=1}} \pi(\mathbf{F}, \mathbf{C}^p, \alpha). \quad (36)$$

Similarly to the time-continuous case, the assumption of $q_n \geq 0$ (Equation (12)) implies that the minimum is achieved for

$$\Delta \alpha = \sqrt{\frac{2}{3}} 1/2 \|\mathbf{c}^p - \mathbf{I}\|, \quad (37)$$

which we can directly insert in Equation (36). Thus, we write for simplicity

$$\inf_{\substack{\mathbf{C}^p \\ \det(\mathbf{C}^p)=1}} \pi(\mathbf{F}, \mathbf{C}^p). \quad (38)$$

2.4 | Treatment of the incompressibility constraint

In the sequel, the focus is on the minimization problems with incompressibility constraint, that is,

$$\inf_{\substack{\mathbf{C}^p \\ \det(\mathbf{C}^p)=1}} \pi_\Delta(\mathbf{F}, \mathbf{C}^p), \quad (39)$$

where we now employ the special-linear update from Hurtado et al.⁹

In order to obtain a constraint-free minimization problem, which is way easier to handle numerically, the unconstrained tensor $\hat{\mathbf{C}}^p$ is introduced via the nonlinear projection

$$\mathbf{C}^p(\hat{\mathbf{C}}^p) = \left(\det(\hat{\mathbf{C}}^p) \right)^{-\frac{1}{3}} \hat{\mathbf{C}}^p. \quad (40)$$

This projection is depicted in Figure 1, where one can see that the unconstrained tensor $\hat{\mathbf{C}}^p$ may change the shape and volume of the body. However, the term $\det(\hat{\mathbf{C}}^p)^{-\frac{1}{3}} \mathbf{I}$ scales back any volumetric stretches that were included in $\hat{\mathbf{C}}^p$. Therefore, this projection intrinsically ensures the unimodularity of \mathbf{C}^p and allows to reformulate the minimization problem in Equation (39) to

$$\inf_{\hat{\mathbf{C}}^p} \pi_\Delta(\mathbf{F}, \mathbf{C}^p(\hat{\mathbf{C}}^p)). \quad (41)$$

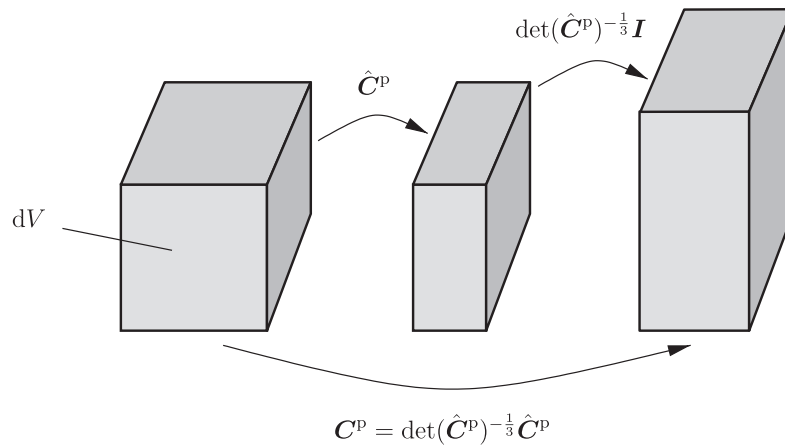


FIGURE 1 Volume dV in the reference configuration is stretched by $\hat{\mathbf{C}}^p$, followed by a volumetric stretch $\det(\hat{\mathbf{C}}^p)^{-\frac{1}{3}}\mathbf{I}$, summarized by \mathbf{C}^p

Obviously, the constraint on \mathbf{C}^p is gone. Unfortunately, the degree-1-homogeneous potential ϕ_Δ is not differentiable at $\mathbf{c}^p = \mathbf{I}$, which makes the numerical solution difficult. For that reason, a further reparametrization of $\hat{\mathbf{c}}^p = \mathbf{U}_n^{p-1}\hat{\mathbf{C}}^p\mathbf{U}_n^{p-1}$ (cf. Equation (33)) is proposed as

$$\mathbf{c}^p = \mathbf{U}_n^{p-1}\mathbf{C}^p\mathbf{U}_n^{p-1} = \hat{\mathbf{I}}^{p-\frac{1}{3}}\hat{\mathbf{c}}^p, \quad (42)$$

$$\hat{\mathbf{c}}^p = \mathbf{I} + 2\Delta\gamma\mathbf{N}^p \rightarrow \hat{\mathbf{C}}^p = \mathbf{C}_n^p + 2\Delta\gamma\mathbf{U}_n^p\mathbf{N}^p\mathbf{U}_n^p, \quad (43)$$

where \mathbf{N}^p is a symmetric tensor with $\|\mathbf{N}^p\| = 1$. Employing this reparametrization into Equation (32)₁ yields

$$\begin{aligned} \phi_\Delta &= \frac{1}{2}\sqrt{\frac{2}{3}}\sigma_{y0}\|\mathbf{c}^p(\hat{\mathbf{c}}^p) - \mathbf{I}\| \\ &= \frac{1}{2}\sqrt{\frac{2}{3}}\sigma_{y0}\|\hat{\mathbf{I}}^{p-\frac{1}{3}}(\mathbf{I} + 2\Delta\gamma\mathbf{N}^p) - \mathbf{I}\|. \end{aligned} \quad (44)$$

Inserting the reparametrization from Equation (42) into Equation (41) results in the minimization problem

$$\inf_{\substack{\Delta\gamma \geq 0, \mathbf{N}^p \\ \|\mathbf{N}^p\| = 1}} \pi_\Delta \left(\mathbf{F}, \mathbf{C}^p \left(\mathbf{U}_n^{p-1}(\mathbf{I} + 2\Delta\gamma\mathbf{N}^p)\mathbf{U}_n^{p-1} \right) \right). \quad (45)$$

In order to eliminate the constraint $\|\mathbf{N}^p\| = 1$, one final reparametrization of \mathbf{N}^p is introduced as

$$\mathbf{N}^p = \frac{\mathbf{U}_n^{p-1}\tilde{\mathbf{N}}^s\mathbf{U}_n^{p-1}}{\|\mathbf{U}_n^{p-1}\tilde{\mathbf{N}}^s\mathbf{U}_n^{p-1}\|}, \quad (46)$$

where $\tilde{\mathbf{N}}^s$ is a symmetric but otherwise unconstrained tensor. Obviously, $\|\mathbf{N}^p\| = 1$ now intrinsically holds. Therefore, inserting this reparametrization into the minimization problem from Equation (45) drops the constraint and yields

$$\inf_{\Delta\gamma \geq 0, \tilde{\mathbf{N}}^s} \pi_\Delta \left(\mathbf{F}, \mathbf{C}^p(\Delta\gamma, \tilde{\mathbf{N}}^s) \right). \quad (47)$$

Now, the minimization in Equation (47) can be accomplished by solving the nonlinear equation set

$$\begin{aligned} \frac{\partial \pi_\Delta}{\partial \mathbf{z}} &= 0 \\ \Rightarrow \frac{\partial \pi_\Delta}{\partial \Delta\gamma} &= 0, \quad \frac{\partial \pi_\Delta}{\partial \tilde{\mathbf{N}}^s} = 0 \end{aligned} \quad (48)$$

with a Newton-scheme. Here, $\mathbf{z} = (\Delta\gamma, \tilde{\mathbf{N}}^s)$ is the set of parametrized internal variables. The entire first and second derivatives employed in the Newton-scheme are summarized in Appendix C and D.

As the observant reader might have already seen, the system matrix $\frac{\partial^2 \pi_\Delta}{\partial \mathbf{z}^2}$ is singular. This is due to the minimization problem being independent of $\det(\hat{\mathbf{C}}^p)$ as well as $\|\tilde{\mathbf{N}}^s\|$. For $\det(\hat{\mathbf{C}}^p)$, this is depicted in Figure 2, where two different $\hat{\mathbf{C}}_i^p$ with different determinants both yield the same tensor \mathbf{C}^p . Therefore, the minimization problem as it stands is not uniquely solvable. In addition, the algorithmic yield criterion is derived in Appendix B.

2.5 | Elimination of singularities

To eliminate the aforementioned singularities introduced through $\det(\hat{\mathbf{C}}^p)$ and $\|\mathbf{N}^p\|$, the regularization potential π_R is introduced as

$$\pi_R = \frac{1}{2}A \left((\hat{\mathbf{m}}^p - 1)^2 + (\|\mathbf{U}_n^{p-1} \tilde{\mathbf{N}}^s \mathbf{U}_n^{p-1}\| - 1)^2 \right), \quad (49)$$

where A is an arbitrary numerical constant. This energy can be interpreted as a spring attached to $\det(\hat{\mathbf{C}}^p)$ and $\|\mathbf{N}^p\|$, pulling on both to be equal to 1. Since π_Δ is otherwise free of $\det(\hat{\mathbf{C}}^p)$ and $\|\mathbf{N}^p\|$, adding this term to π_Δ ensures that in the converged solution state $\det(\hat{\mathbf{C}}^p) = 1$ as well as $\|\mathbf{N}^p\| = 1$ are *exactly* satisfied. Therefore, it is emphasized that the constant A has no influence on the solution for $\{\mathbf{C}^p, \alpha\}$, since $\pi_R = 0$ holds in the converged state.

2.6 | Improving the approximation of the logarithm

The approximation used in Equation (32) is only first-order accurate. A higher accuracy can be achieved using the logarithm (see Section 2.3). This is depicted in Figure 3, where the approximation of the logarithm is compared to the logarithm itself for the first two eigenvalues of $\Delta\mathbf{c}^p$. Here, $\Delta\mathbf{c}^p$ is calculated as

$$\Delta\mathbf{c}^p = \mathbf{c}^p - \mathbf{I}. \quad (50)$$

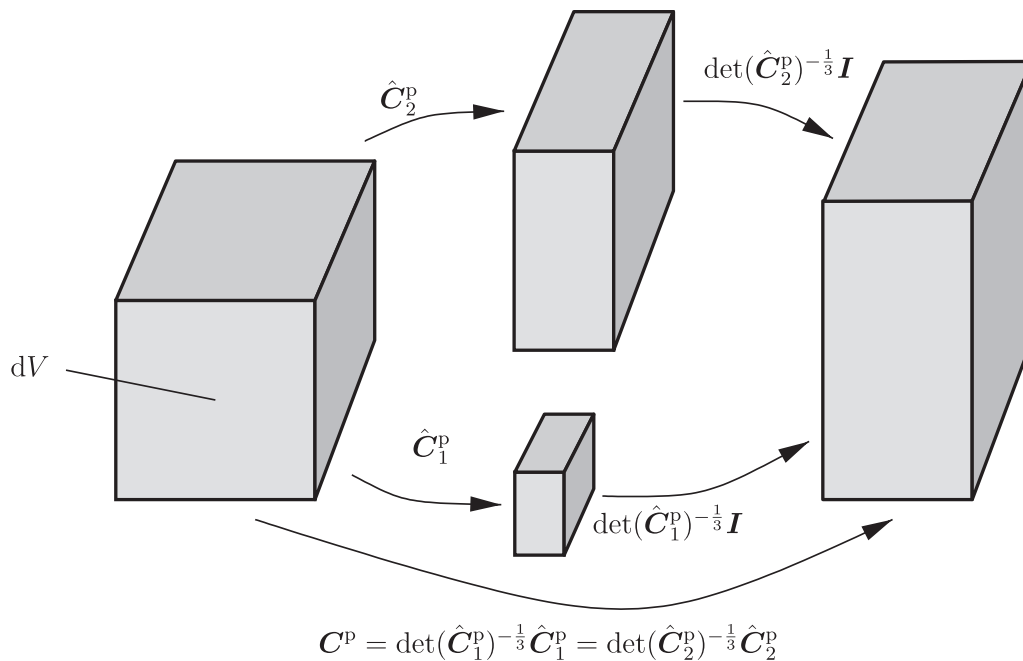


FIGURE 2 Volume dV in the reference configuration is stretched by either $\det(\hat{\mathbf{C}}_1^p)$ or $\det(\hat{\mathbf{C}}_2^p)$, followed by a volumetric stretch $\det(\hat{\mathbf{C}}_1^p)^{-\frac{1}{3}}\mathbf{I}$ and $\det(\hat{\mathbf{C}}_2^p)^{-\frac{1}{3}}\mathbf{I}$, respectively. However, both yield the same \mathbf{C}^p

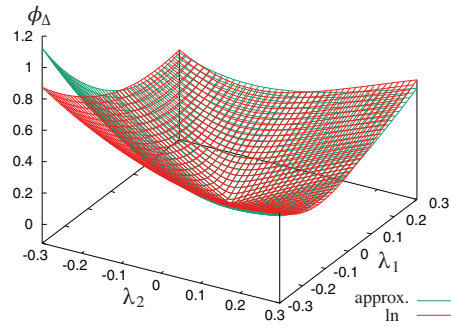


FIGURE 3 Comparison of ϕ_Δ using the approximation (cf. Equation (32)) and the logarithm

Furthermore, the third eigenvalue is also accounted for using the constraint $\det(\mathbf{c}^p) = 1$:

$$\rightarrow (1 + \lambda_1)(1 + \lambda_2)(1 + \lambda_3) = 1 \rightarrow \lambda_3 = \frac{1}{(1 + \lambda_1)(1 + \lambda_2)} - 1. \quad (51)$$

As one can see, the approximation is very close to the logarithm when $\Delta \mathbf{c}^p$ is small. However, as the eigenvalues of $\Delta \mathbf{c}^p$ get larger, which correspond to larger load-steps, the error drastically increases. Therefore, the approximation of the logarithm is improved using the first two invariants of $\Delta \mathbf{c}^p$. For the improved approximation of the dissipation potential we use the ansatz

$$\phi_\Delta = \sqrt{\frac{2}{3}} \sigma_{y0} \left(\left\| \frac{1}{2} (\mathbf{c}^p - \mathbf{I}) \right\| + a_1 \mathbf{I}_{\Delta \mathbf{c}^p} + a_2 \mathbf{II}_{\Delta \mathbf{c}^p} \right), \quad (52)$$

where a_1 and a_2 are constants. In the context of this article, they are optimized by a least-squares algorithm, minimizing the difference to the logarithmic approximation, as $a_1 = 3.0$ and $a_2 = 3.1$. For the least-squares algorithm, 21x21 equidistant support points over the range of $\lambda_1 \in [-0.25, 0.25]$ and $\lambda_2 \in [-0.25, 0.25]$ are used. Further, $\mathbf{I}_{\Delta \mathbf{c}^p}$ and $\mathbf{II}_{\Delta \mathbf{c}^p}$ are the first and second invariants of $\Delta \mathbf{c}^p$, respectively. Here it is important to note, that this modification is time consistent, that is, $\phi_\Delta \rightarrow 0$ for $\Delta t \rightarrow 0$. The improved approximation is compared to the old approximation and the logarithm in Figure 4 for the eigenvalues of $\Delta \mathbf{c}^p$. Clearly the improved approximation is closer to the natural logarithm, even for larger eigenvalues of $\Delta \mathbf{c}^p$. Therefore, the improved approximation enables better results for larger time steps. This is shown in Section 3.3, where the results for the initial approximation are compared to the ones of the improved approximation.

2.7 | Initial guesses for $\Delta \gamma$ and \tilde{N}^s

In this article, a Newton-scheme is chosen to minimize the discretized potential. Therefore, good initial guesses for the unknowns are required to ensure that a solution can be found. For the initial guess of $\Delta \gamma$, the choice of $\Delta \gamma_0 = 0$ proves to

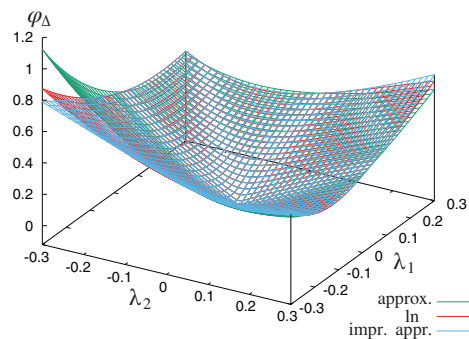


FIGURE 4 Comparison of ϕ_Δ using the approximation (cf. Equation (32)), the improved approximation (cf. Equation (52)) and the logarithm

be advantageous. Then, one can solve

$$\mathbf{N}_0^p = \arg \inf_{\substack{\mathbf{N}^p \\ \|\mathbf{N}^p\|=1}} \lim_{\Delta\gamma \rightarrow 0} \pi_\Delta \quad (53)$$

to obtain a good initial guess for $\tilde{\mathbf{N}}^s$ (cf. Equation (45)). This leads to

$$\mathbf{N}_0^p = \frac{\sum_{\text{tr}}^{\text{eff}} \mathbf{C}_n^p}{\|\sum_{\text{tr}}^{\text{eff}} \mathbf{C}_n^p\|}, \quad (54)$$

where $\sum_{\text{tr}}^{\text{eff}}$ is the trial value of Σ^{eff} (see Equation (28)), defined as

$$\sum_{\text{tr}}^{\text{eff}} = \mathbf{F}^{\text{etr}\top} \boldsymbol{\tau}^{\text{tr}} \mathbf{F}^{\text{etr}-1} - \Sigma_n^{\text{b}'}. \quad (55)$$

Here, $\boldsymbol{\tau}^{\text{tr}}$ is the Kirchhoff stress evaluated with the trial value $\mathbf{b}^{\text{etr}} = \mathbf{F}^{\text{etr}\top} \mathbf{F}^{\text{etr}}$, where $\mathbf{F}^{\text{etr}} = \mathbf{F} \mathbf{F}_n^{p-1}$. With the initial guesses defined, the ingredients for the solution of the minimization problem are altogether.

2.8 | Solving the local and global system of equations

The local minimization scheme is embedded in the global minimization problem, where one minimizes

$$\Pi_\Delta = \int_{\Omega_0} \pi_\Delta d\Omega - \int_{\partial\Omega_{0t}} \hat{\mathbf{t}} \cdot \mathbf{u} dS. \quad (56)$$

Here, $\hat{\mathbf{t}}$ is the traction vector acting on the surface $\partial\Omega_{0t} \subset \partial\Omega_0$ of the reference configuration Ω_0 and \mathbf{u} is the displacement vector. Additionally, body forces are neglected for simplicity. To minimize this global problem, the consistent tangent is required, which is given in Appendix E. Additionally, the Newton scheme solving the local minimization problem is summarized in Algorithm 1.

3 | NUMERICAL RESULTS FOR ISOTROPIC HARDENING

In this section, the presented model is tested for convergence with respect to step size Δt and compared to results from Simo.¹⁷

Algorithm 1. Newton scheme solving the equation set in Eq. (48)

```

Compute trial variables  $\mathbf{F}^{\text{etr}}, \boldsymbol{\tau}^{\text{tr}}$ 
Compute yield criterion  $f$ 
if  $f^{\text{tr}} \geq 0$  then
     $\boldsymbol{\tau} = \boldsymbol{\tau}^{\text{tr}}, \mathbf{C}^p = \mathbf{C}_n^p, \alpha = \alpha_n$ 
    Compute algorithmic tangent  $\mathbb{C}^{\text{algo}}$ 
else
    while  $\left\| \frac{\partial \pi_\Delta}{\partial \mathbf{z}} \right\| \geq \text{tol}^{\text{Nwt n}}$  do
        Compute  $\mathbf{N}^p, \hat{\mathbf{C}}^p, \mathbf{C}^p, \mathbf{b}^c, \Delta\alpha, \boldsymbol{\tau}, \mathbf{C}^{\text{pd}}$ 
        Compute Residual  $\frac{\partial \pi_\Delta}{\partial \mathbf{z}}$  and system matrix  $\frac{\partial^2 \pi_\Delta}{\partial \mathbf{z}^2}$ 
        Solve  $\frac{\partial^2 \pi_\Delta}{\partial \mathbf{z}^2} \Delta \mathbf{z} = -\frac{\partial \pi_\Delta}{\partial \mathbf{z}}$  for  $\Delta \mathbf{z}$ 
    end while
    Compute algorithmic tangent  $\mathbb{C}^{\text{algo}}$ 
end if

```

3.1 | Gauss point evaluations

To investigate the model implementation and convergence of the occurring stresses with regard to step size Δt , Gauss point evaluations are conducted. Therefore, the response of the material for a single Gauss-point in case of cyclic uniaxial tension and compression as well as simple shear was investigated. The deformation was prescribed by incrementally increasing and decreasing F while preserving the volume of the Gauss-point. Figures 5 and 6 show the comparison of stresses for different amounts of equidistant load steps for uniaxial tension and simple shear, respectively. Due to the lack of an analytical solution, the solutions can only be compared to a converged solution with many load steps. As one can see, the error in comparison to the converged solution obtained is very small. For tension and compression, even for only 50 steps, σ_{11} deviates by less than 0.5%. Here, it is noted that the largest difference lies in the elastic regime and only stems from the fact that the second evaluation is already far in the plastic regime. Further, for simple shear the error in the final shear stress is less than 1% for only 50 steps. Having evaluated the robustness and convergence behavior of the model, now a 3D problem is investigated.

3.2 | 3D necking of a circular bar

To validate the model results in 3D, the necking of a circular bar proposed by Simo¹⁷ is compared to this model results.

A circular bar with radius $r_0 = 6.413$ mm of length $l = 53.334$ mm is subjected to a displacement controlled pure tension test using simple support boundary conditions. To prevent bifurcation, the cross-section is reduced in the middle

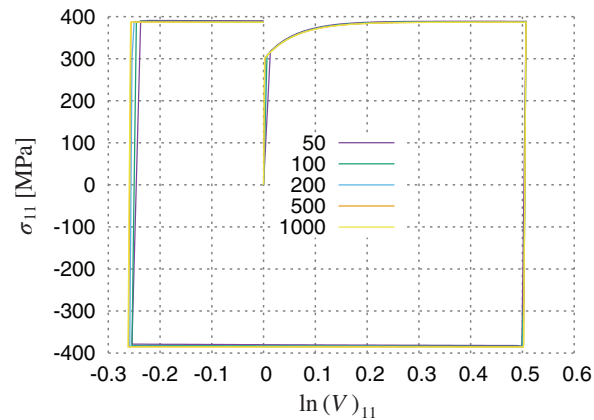


FIGURE 5 Stress σ_{11} over strain $\ln(V)_{11}$ in a tensile test for different numbers of time steps

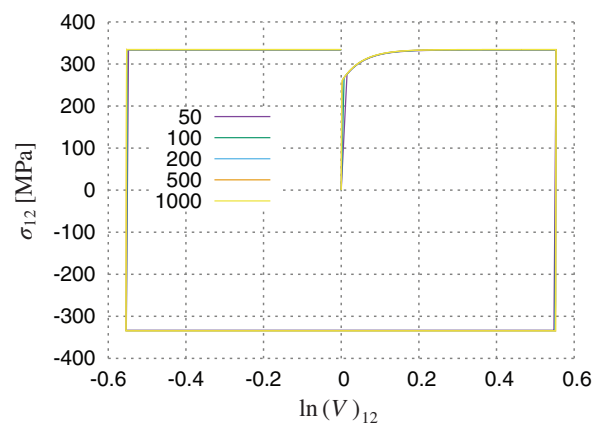


FIGURE 6 Stress σ_{12} over strain $\ln(V)_{12}$ in a simple shear test for different numbers of time steps

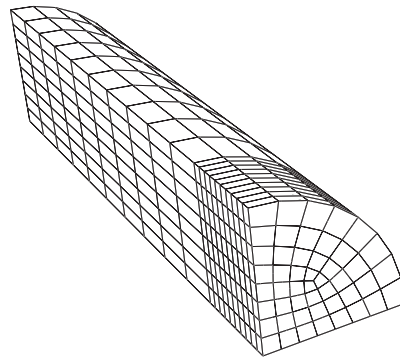


FIGURE 7 Mesh of the circular bar with 960 Q1/P0 elements used in simulation

of the bar, as described in Reference 17. Due to the obvious symmetries, only one eighth of the bar is analyzed, which is shown in Figure 7. This boundary value problem as well as the additional 3D-Problem in Section 4 are solved using the finite element analysis program FEAP.¹⁸ For this problem, the isotropic hardening energy ψ_h is chosen to be of the Voce-type as

$$\frac{\partial \psi_h}{\partial \alpha} = H\alpha + (\sigma_{y0} - \sigma_y)(1 - \exp(-\beta\alpha)), \quad (57)$$

like in Simo.¹⁷ Likewise, the elastic and isotropic hardening material parameters were chosen accordingly, which are given in Table 1. Further, the numerical parameters are aggregated in Table 2. Here, $\tau_{01}^{Nwt^n}$ is the tolerance of the local Newton scheme presented in Algorithm 1. The deformed bar is shown in Figure 8. Now, the influence of the number of equidistant time steps is evaluated. The necking displacement is plotted against the elongation for a varying number of time steps in Figure 9. Clearly, the final necking displacement converges to a value of roughly 3.8 mm.

TABLE 1 Material parameters for necking of a circular bar

κ [MPa]	μ [MPa]	σ_y [MPa]	$\sigma_{y\infty}$ [MPa]	β	H [MPa]
164,210	80,193.8	450	715	16.93	129.24

TABLE 2 Numerical parameters for necking of a circular bar

$\tau_{01}^{Nwt^n}$ [-]	A [MPa]	α_1 [MPa]	α_2 [MPa]
10^{-8}	10^4	3.0	3.1

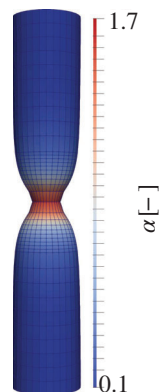


FIGURE 8 Distribution of the equivalent plastic strain α over the deformed bar after loading

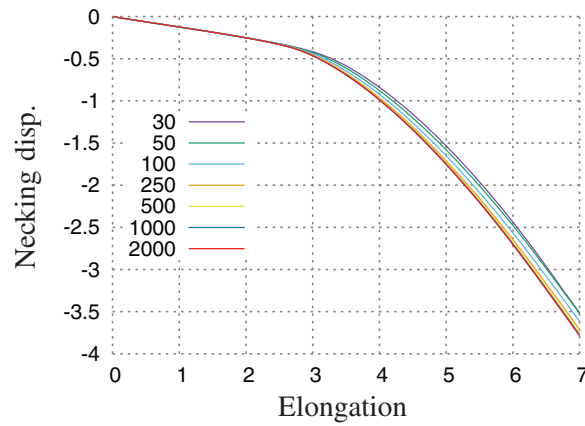


FIGURE 9 Necking displacement versus elongation for varying amounts of time steps using the improved logarithms approximation

3.3 | Comparison of the approximations of the logarithm

In this section, the results of the original first-order approximation of ϕ_Δ (Equation (32)) and its improved counterpart (Equation (52)), introduced in Section 2.6, are compared. To illustrate the difference in the convergence behavior, the same problem as in the previous section is run again with the approximation omitting the invariants. The results are shown in Figure 10. While the results, in comparison to the ones in the previous section, clearly converge toward the same displacement, the results for smaller numbers of time steps clearly improved. Therefore, it can be concluded that the improved approximation utilizing the invariances improved the model results by a large margin for not fully converged results with regard to time steps.

4 | INCORPORATION OF KINEMATIC HARDENING

4.1 | Expanding the potential for kinematic hardening

To expand the time discrete counterpart π_Δ for kinematic hardening, ψ_k is replaced by its algorithmic counterpart $\tilde{\psi}_k$, which is defined as

$$\tilde{\psi}_k = \mu^p \Delta C^p : C_{n+\frac{1}{2}}^{pd-1}. \quad (58)$$

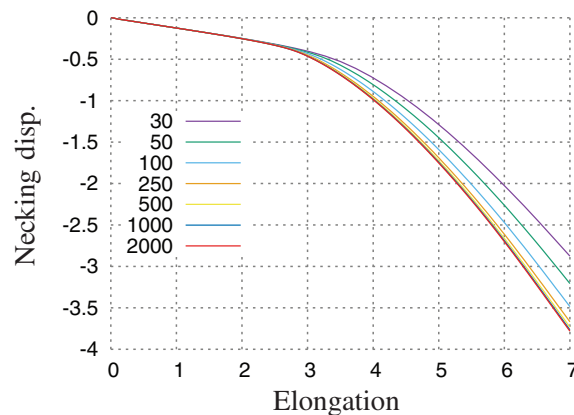


FIGURE 10 Necking displacement versus elongation for varying amounts of time steps using the logarithm approximation without the invariants

Here, in comparison to ψ_k from Equation (13), ΔC^p is used instead of C^p , because using C^p leads to $\tilde{\psi}_k$ being not consistent with the time-continuous case. Additionally, it turned out that using the midpoint evaluation

$$C_{n+\frac{1}{2}}^{pd-1} = \frac{1}{2} \left(C_n^{pd-1} + C^{pd-1} \right) \quad (59)$$

instead of C^{pd-1} leads to more accurate results. Further, in line with Equation (40), C^{pd} is reparametrized to be unimodular:

$$C^{pd} = \left(\det \left(\hat{C}^{pd} \right) \right)^{-\frac{1}{3}} \hat{C}^{pd}. \quad (60)$$

Then again, since we assume a Frederick–Armstrong hardening law, \hat{C}^{pd} is defined depending on the plastic multiplier γ as

$$\hat{C}^{pd} = C_n^{pd} + 2\Delta\gamma \frac{b}{c} \Sigma_n^{b'}. \quad (61)$$

Incorporating $\tilde{\psi}_k$ into the discretized potential π_Δ yields

$$\pi_\Delta = \psi_e + \psi_h + \tilde{\psi}_k - (\psi_{e_n} + \psi_{h_n} + \tilde{\psi}_{k_n}) + \phi_\Delta. \quad (62)$$

In the following subsection, this potential is minimized with respect to $\Delta\gamma$ and \tilde{N}^s , again.

4.2 | Results for kinematic hardening

To validate the results of the kinematic hardening extension, the model results were compared to the results in Vladimirov et al.⁷ Therefore, the material parameters in Table 3 are adapted, which also partially originate from Lührs et al.¹⁹ Likewise, the isotropic hardening energy adopted from Vladimirov et al.⁷ is of Voce-type and reads

$$\psi_h = Q \left(\alpha + \frac{\exp(-\beta\alpha)}{\beta} \right). \quad (63)$$

First, the stress-strain Gauss-point computations in tension-compression as well as simple shear are shown in Figures 11 and 12. Again, as in the isotropic hardening section, one can clearly see the results converging for an increasing number of time steps per load cycle. Further, since there is not an analytical solution, the results are compared to the results from Vladimirov et al.⁷ Here, one can see, that the error introduced by only using 50 time steps is very small in both tests. Additionally, the Bauschinger effect, which changes the yield stress depending on the direction of load, is clearly visible in both tests. Further, the results for the shear test compare well with Vladimirov et al.⁷

Next, the 3D finite element example from Vladimirov et al.⁷ was used to validate the results of the model. A cube with a side length of 1 mm is loaded by a combined tensile and shear loading. At the bottom of the cube, a boundary condition holds all degrees of freedom, while on the top a displacement boundary condition is prescribed in two steps for the displacements u_1 and u_2 as

$$\begin{aligned} \text{Step 1 : } & u_1 = 1 \text{ mm}, & u_2 = 0.5 \text{ mm}, \\ \text{Step 2 : } & u_1 = -1 \text{ mm}, & u_2 = 0.5 \text{ mm}. \end{aligned}$$

The cube is discretized by four different regular meshes with 8, 64, 512, 1728, and 4096 Q1P0 elements. Due to the obvious symmetries, only one quarter of the cube has to be modeled. The cube is shown in an almost undeformed state,

TABLE 3 Parameters for kinematic hardening from Lührs et al.¹⁹ and Vladimirov et al.⁷

μ [MPa]	λ [MPa]	σ_y [MPa]	Q [MPa]	β	μ^p [MPa]	c [MPa]	b
80,000	119,999.67	300	400	2.5	950	1900	8.5

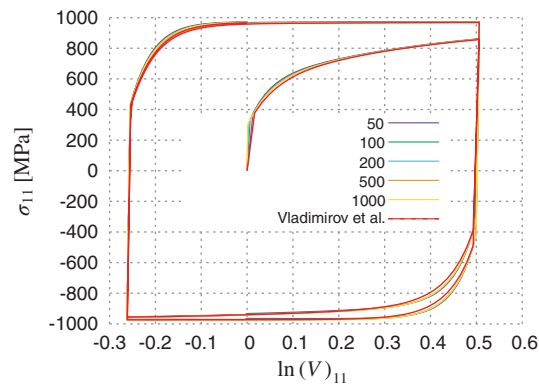


FIGURE 11 Stress σ_{11} over strain $\ln(V)_{11}$ in a tensile test for different numbers of time steps in comparison to Vladimirov et al.⁷

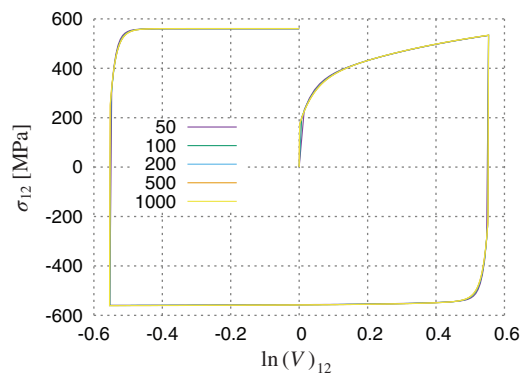


FIGURE 12 Stress σ_{12} over strain $\ln(V)_{12}$ in a simple shear test for different numbers of time steps

after load *step 1* and after load *step 2* in Figure 13. Obviously, these large deformations are uncharacteristic for a metal cube. However, as stated in Vladimirov et al.,⁷ it serves well as a test showing the model's capabilities in the finite strain regime. The convergence of the stresses in the middle of the cube after load *step 1* with regard to the amount of time steps is shown in Figure 14. Here, the finest discretization with 4096 finite elements is used. Clearly, one can see the stresses quickly converging toward 962 N/mm² for the finer meshes. Only for the mesh with just eight elements the results are deviating far from the converged solution.

Next, the convergence of the stresses in the middle of the cube after load *step 1* of the cube with regard to the cube discretization is investigated. Therefore, the variously fine discretized meshes are all loaded in 1000 steps. The resulting stresses are shown in Figure 15. Again, the values converge for decreasing time steps. However, in contrast to Vladimirov

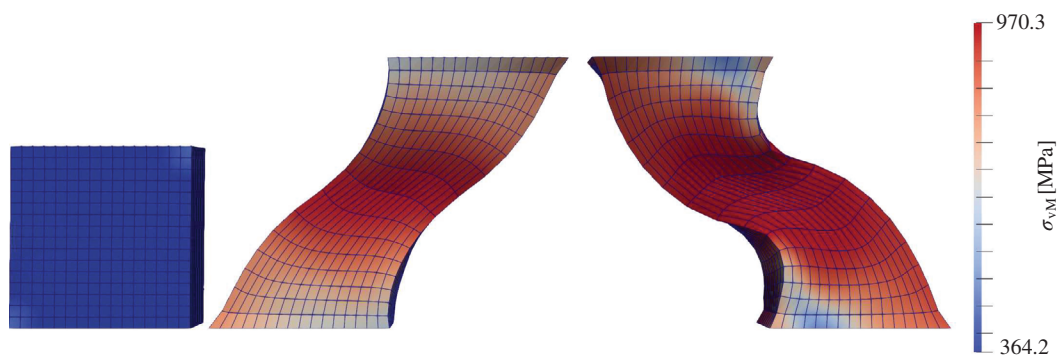


FIGURE 13 Deformed cube from left to right: Almost undeformed, after load *step 1* and after load *step 2*

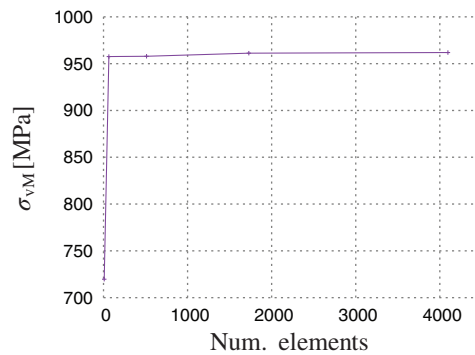


FIGURE 14 Convergence of the stress in the middle of the cube after *step 1* with regards to the amount of finite elements

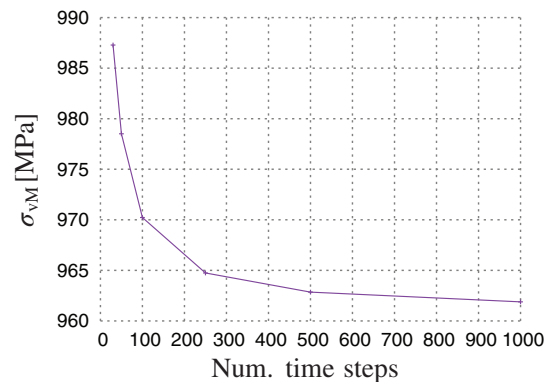


FIGURE 15 Convergence of the stress in the middle of the cube after *step 1* with regards to the number of time steps

et al.,⁷ the results converge strictly from above toward their final value. Overall, while being quite satisfying, the time convergence behavior of this model is not as good as that of the exponential mapping approach.

5 | SUMMARY AND OUTLOOK

In this article, a numerical approach for the solution of large deformation elastoplasticity is presented. In contrast to many recent works, it does not use the exponential map to fulfill the incompressibility constraint. The model is formulated in the generalized standard materials framework to ensure thermodynamic consistency. Further, the model was extended to kinematic hardening in Section 4. The model's capability of producing reasonable results in both isotropic and kinematic hardening is shown through numerical experiments. The time convergence behavior for isotropic hardening was improved using an ansatz involving the invariants of c^p . This improvement is enabled by having the possibility for a flexible modification of the time-discretized potentials, which opens the door for further improvements like the control of the convexity of the potential or potential-based line search algorithms. In the future, it should be investigated how to improve the accuracy for large time steps for kinematic hardening. In this case, the proposed model is still clearly inferior to the exponential map. However, it comes with the advantage of inherently having symmetric internal variables for kinematic hardening without any modifications to the approach. This is not the case for the exponential map, where it proved to be a tedious task, as can be seen from the publication history on that topic (e.g., Dettmer and Reese,⁶ Vladimirov et al.⁷). For these reasons, it remains very interesting to also employ this model in more complicated inelastic models, for example, shape memory alloys, where the usage of the exponential map may also be involved.

ACKNOWLEDGMENTS

Financial support of subproject A3 *Cooperative Actuator Systems for Nanomechanics and Nanophotonics: Coupled Simulation* of the Priority Programme SPP 2206 by the German Research Foundation (DFG) (Grant WU847/3-1) is gratefully

acknowledged by Marian Sielenkämper and Stephan Wulfinghoff. Funding by the German Research Foundation (DFG) for the project P12 within the framework of the research training group GRK 2154 “Materials for Brain: Thin film functional materials for minimally invasive therapy of brain diseases” (Grant GRK 2154/1) is gratefully acknowledged by Stephan Wulfinghoff and Jan Dittmann.

DATA AVAILABILITY STATEMENT

Data, specifically the code used to generate the results, is openly available in a public repository that issues datasets with DOIs.

Data openly available in a public repository that issues datasets with DOIs.

ORCID

Marian Sielenkämper  <https://orcid.org/0000-0002-5884-1588>

Jan Dittmann  <https://orcid.org/0000-0001-5519-0647>

REFERENCES

1. Eckart C. The thermodynamics of irreversible processes. IV. the theory of elasticity and anelasticity. *Phys Rev.* 1948;73(4):373.
2. Kröner E. Allgemeine Kontinuumstheorie der Versetzungen und Eigenspannungen. *Arch Ration Mech Anal.* 1959;4(1):273.
3. Lee EH. Elastic-plastic deformation at finite strains; 1969:1-6.
4. Weber G, Anand L. Finite deformation constitutive equations and a time integration procedure for isotropic, hyperelastic-viscoplastic solids. *Comput Methods Appl Mech Eng.* 1990;79(2):173-202.
5. Miehe C. Exponential map algorithm for stress updates in anisotropic multiplicative elastoplasticity for single crystals. *Int J Numer Methods Eng.* 1996;39(19):3367-3390.
6. Dettmer W, Reese S. On the theoretical and numerical modelling of Armstrong–Frederick kinematic hardening in the finite strain regime. *Comput Methods Appl Mech Eng.* 2004;193(1-2):87-116.
7. Vladimirov IN, Pietryga MP, Reese S. On the modelling of non-linear kinematic hardening at finite strains with application to springback–Comparison of time integration algorithms. *Int J Numer Methods Eng.* 2008;75(1):1-28.
8. Ortiz M, Radovitzky R, Repetto E. The computation of the exponential and logarithmic mappings and their first and second linearizations. *Int J Numer Methods Eng.* 2001;52(12):1431-1441.
9. Hurtado DE, Stainier L, Ortiz M. The special-linear update: an application of differential manifold theory to the update of isochoric plasticity flow rules. *Int J Numer Methods Eng.* 2014;97(4):298-312.
10. Yoshida F, Uemori T. A model of large-strain cyclic plasticity and its application to springback simulation. *Int J Mech Sci.* 2003;45(10):1687-1702.
11. Tong J, Zhan ZL, Vermeulen B. Modelling of cyclic plasticity and viscoplasticity of a nickel-based alloy using Chaboche constitutive equations. *Int J Fatigue.* 2004;26(8):829-837.
12. Lion A. Constitutive modelling in finite thermoviscoplasticity: a physical approach based on nonlinear rheological models. *Int J Plasticity.* 2000;16(5):469-494.
13. Armstrong PJ, Frederick C. *A Mathematical Representation of the Multiaxial Bauschinger Effect.* Vol 731. Central Electricity Generating Board; 1966.
14. Halphen B, Nguyen QS. Sur les matériaux standard généralisés; 1975.
15. Han W, Reddy BD. *Plasticity: Mathematical Theory and Numerical Analysis.* Vol 9. Springer Science & Business Media; 1999.
16. Ortiz M, Stainier L. The variational formulation of viscoplastic constitutive updates. *Comput Methods Appl Mech Eng.* 1999;171(3-4):419-444.
17. Simo JC. Algorithms for static and dynamic multiplicative plasticity that preserve the classical return mapping schemes of the infinitesimal theory. *Comput Methods Appl Mech Eng.* 1992;99(1):61-112.
18. Taylor RL. FEAP - finite element analysis program; 2017. <http://projects.ce.berkeley.edu/feap/>
19. Lührs G, Hartmann S, Haupt P. On the numerical treatment of finite deformations in elastoviscoplasticity. *Comput Methods Appl Mech Eng.* 1997;144(1-2):1-21.

How to cite this article: Sielenkämper M, Dittmann J, Wulfinghoff S. Numerical strategies for variational updates in large strain inelasticity with incompressibility constraint. *Int J Numer Methods Eng.* 2022;123(1):245-267. doi: 10.1002/nme.6855

APPENDIX A. CONSISTENCY OF THE DISSIPATION POTENTIAL

To solve the boundary value problem, one wants to find an algorithmic counterpart to ϕ , which is ϕ_Δ , where the rate-type quantities \mathbf{D}^p and $\dot{\alpha}$ are expressed in terms of the increments of the internal variables in a time step from t_n to t_{n+1} . The algorithmic approximation of ϕ must be consistent, that is,

$$\phi = \lim_{\Delta t \rightarrow 0} \frac{1}{\Delta t} \phi_\Delta. \quad (\text{A1})$$

APPENDIX B. ALGORITHMIC YIELD CRITERION

In order to decide whether a time step is elastic or plastic, we consider the trial state $\pi_\Delta(\mathbf{F}, \mathbf{C}_n^p)$. Then, we apply an infinitesimal increment

$$d\mathbf{C}^p = d\gamma \mathbf{U}_n^p \mathbf{N}^p \mathbf{U}_n^p \quad (d\gamma \geq 0) \quad (\text{B1})$$

and test if

$$\pi_\Delta(\mathbf{F}, \mathbf{C}_n^p + d\mathbf{C}^p) < \pi_\Delta(\mathbf{F}, \mathbf{C}_n^p). \quad (\text{B2})$$

If this is true for any deviatoric direction \mathbf{N}^p , the step is plastic, otherwise it is elastic. Equation (B2) is equivalent to $f \leq 0$, that is, it is sufficient to check the usual yield criterion. The proof is in analogy to the time-continuous case.

APPENDIX C. FIRST DERIVATIVES OF π_Δ

To minimize the discretized potential, one needs the first and second derivatives of the discretized potential with respect to the internal variables. To obtain a more compact notation, \mathbf{N}^s is introduced as

$$\mathbf{N}^s = \mathbf{C}_n^p \mathbf{N}^p. \quad (\text{C1})$$

Additionally, \mathbb{I}^s is the fourth order identity on symmetric matrices. Further, the total yield stress σ_y is given by

$$\sigma_y = \sigma_{y0} + \frac{\partial \psi_h}{\partial \alpha}. \quad (\text{C2})$$

Furthermore, the symmetrizing box product is defined via

$$\mathbf{A} \square^s \mathbf{B} : \mathbf{C} = \text{Asym}^s(\mathbf{C}) \mathbf{B}. \quad (\text{C3})$$

The first derivatives of the discretized potential w.r.t. the internal variables are given by

$$\begin{aligned} d\pi_\Delta = \boldsymbol{\tau} : d\mathbf{d} &+ \underbrace{\left(\frac{\partial(\psi_e + \tilde{\psi}_k)}{\partial \hat{\mathbf{C}}^p} : 2\mathbf{N}^s + \frac{\partial \tilde{\psi}_k}{\partial \hat{\mathbf{C}}^{pd}} : 2 \frac{b}{a} \boldsymbol{\Sigma}_n^{b'} \mathbf{C}_n^{pd} + \sigma_y \frac{\partial \Delta \alpha}{\partial \Delta \gamma} + \frac{\partial \pi_R}{\partial \hat{\mathbf{m}}^p} \hat{\mathbf{m}}^p \hat{\mathbf{C}}^{p-1} : 2\mathbf{N}^s \right)}_{\frac{\partial \pi_\Delta}{\partial \Delta \gamma}} d\Delta \gamma \\ &+ \underbrace{\left[\mathbb{P}_{N^s}^\top : \left(\overbrace{\left(2\Delta \gamma \frac{\partial(\psi_e + \tilde{\psi}_k)}{\partial \hat{\mathbf{C}}^p} + \sigma_y \frac{\partial \Delta \alpha}{\partial N^s} + 2\Delta \gamma \frac{\partial \pi_R}{\partial \hat{\mathbf{m}}^p} \hat{\mathbf{m}}^p \hat{\mathbf{C}}^{p-1} \right)}^{:=A} + \frac{\partial \pi_R}{\partial \tilde{N}^s} \right)}_{\frac{\partial \pi_\Delta}{\partial N^s}} : d\tilde{N}^s. \right]}_{\frac{\partial \pi_\Delta}{\partial N^s}} \end{aligned} \quad (\text{C4})$$

Here, the projector \mathbb{P}_N^s is defined as

$$\mathbb{P}_N^s = \frac{\partial \mathbf{N}^s}{\partial \tilde{\mathbf{N}}^s} = \frac{1}{\|\mathbf{U}_n^{p-1} \tilde{\mathbf{N}}^s \mathbf{U}_n^{p-1}\|} \left(\mathbb{I}^s - \mathbf{N}^s \otimes \mathbf{C}_n^{p-1} \mathbf{N}^s \mathbf{C}_n^{p-1} \right). \quad (\text{C5})$$

Likewise, the projectors \mathbb{P}_p and \mathbb{P}_{pd} are defined as

$$\mathbb{P}_p = \frac{\partial \mathbf{C}^p}{\partial \hat{\mathbf{C}}^p} = \hat{\mathbf{m}}^{p-\frac{1}{3}} \left(\mathbb{I}^s - \frac{1}{3} \hat{\mathbf{C}}^p \otimes \hat{\mathbf{C}}^{p-1} \right), \quad (\text{C6})$$

$$\mathbb{P}_{pd} = \frac{\partial \mathbf{C}^{pd}}{\partial \hat{\mathbf{C}}^{pd}} = \hat{\mathbf{m}}^{pd-\frac{1}{3}} \left(\mathbb{I}^s - \frac{1}{3} \hat{\mathbf{C}}^{pd} \otimes \hat{\mathbf{C}}^{pd-1} \right). \quad (\text{C7})$$

The other occurring derivatives are given as

$$\frac{\partial(\psi_e + \tilde{\psi}_k)}{\partial \hat{\mathbf{C}}^p} = \mathbb{P}_p^\top : \left(-\mathbf{C}^{p-1} \mathbf{F}^T \frac{\partial \psi_e}{\partial \mathbf{b}^e} \mathbf{F} \mathbf{C}^{p-1} + \frac{\mu^p}{2} \left(\mathbf{C}_n^{pd-1} + \mathbf{C}^{pd-1} \right) \right), \quad (\text{C8})$$

$$\frac{\partial \psi_e}{\partial \mathbf{b}^e} = \left(\frac{\lambda}{4} (\det(\mathbf{b}^e) - 1) - \frac{\mu}{2} \right) \mathbf{b}^{e-1} + \frac{\mu}{2} \mathbf{I}, \quad (\text{C9})$$

$$\frac{\partial \tilde{\psi}_k}{\partial \hat{\mathbf{C}}^{pd}} = -\mathbb{P}_{pd}^\top : \frac{1}{2} \mu^p \mathbf{C}^{pd-1} \Delta \mathbf{C}^p \mathbf{C}^{pd-1}, \quad (\text{C10})$$

$$\begin{aligned} \mathbf{M}_{C^p} &:= \frac{\partial (\|\Delta \mathbf{C}^p\| + a_1 \mathbf{I}_{\Delta C^p} + a_2 \mathbf{II}_{\Delta C^p})}{\partial \mathbf{C}^p} \\ &= \frac{\mathbf{C}_n^{p-1} \Delta \mathbf{C}^p \mathbf{C}_n^{p-1}}{\|\mathbf{U}_n^{p-1} \Delta \mathbf{C}^p \mathbf{U}_n^{p-1}\|} \\ &\quad + a_1 \mathbf{C}_n^{p-1} + a_2 \left((\Delta \mathbf{C}^p : \mathbf{C}_n^{p-1}) \mathbf{C}_n^{p-1} - \mathbf{C}_n^{p-1} \Delta \mathbf{C}^p \mathbf{C}_n^{p-1} \right), \end{aligned} \quad (\text{C11})$$

$$\frac{\partial \Delta \alpha}{\partial \Delta \gamma} = \sqrt{\frac{2}{3}} \frac{1}{2} \mathbf{M}_{C^p} : \mathbb{P}_p : 2\mathbf{N}^s, \quad (\text{C12})$$

$$\frac{\partial \pi_R}{\partial \hat{\mathbf{m}}^p} = A(\hat{\mathbf{m}}^p - 1), \quad (\text{C13})$$

$$\frac{\partial \Delta \alpha}{\partial \mathbf{N}^s} = \sqrt{\frac{2}{3}} 2\Delta \gamma \mathbb{P}_p^\top : \frac{1}{2} \mathbf{M}_{C^p}, \quad (\text{C14})$$

$$\frac{\partial \pi_R}{\partial \tilde{\mathbf{N}}^s} = A(\|\mathbf{U}_n^{p-1} \tilde{\mathbf{N}}^s \mathbf{U}_n^{p-1}\| - 1) \left(\frac{\mathbf{C}_n^{p-1} \tilde{\mathbf{N}}^s \mathbf{C}_n^{p-1}}{\|\mathbf{U}_n^{p-1} \tilde{\mathbf{N}}^s \mathbf{U}_n^{p-1}\|} \right). \quad (\text{C15})$$

APPENDIX D. SECOND DERIVATIVES OF π_Δ

The second derivatives of the discretized potential w.r.t. the internal variables are given by

$$\begin{aligned} \frac{\partial^2 \pi_\Delta}{\partial \Delta \gamma^2} &= 2\mathbf{N}^s : \frac{\partial^2(\psi_e + \tilde{\psi}_k)}{\partial \hat{\mathbf{C}}^{p2}} : 2\mathbf{N}^s + 2\mathbf{N}^s : \frac{\partial^2 \pi_R}{\partial \hat{\mathbf{C}}^{p2}} : 2\mathbf{N}^s \\ &\quad + \left(2 \frac{b}{a} \boldsymbol{\Sigma}_n^{b'} \mathbf{C}_n^{pd} \right) : \frac{\partial^2 \tilde{\psi}_k}{\partial \hat{\mathbf{C}}^{pd2}} : \left(2 \frac{b}{a} \boldsymbol{\Sigma}_n^{b'} \mathbf{C}_n^{pd} \right) + \sigma_y \frac{\partial^2 \Delta \alpha}{\partial \Delta \gamma^2} \\ &\quad + 2 \cdot 2\mathbf{N}^s : \frac{\partial^2 \tilde{\psi}_k}{\partial \hat{\mathbf{C}}^p \partial \hat{\mathbf{C}}^{pd}} : \left(2 \frac{b}{a} \boldsymbol{\Sigma}_n^{b'} \mathbf{C}_n^{pd} \right) + \frac{\partial^2 \psi_h}{\partial \alpha^2} \left(\frac{\partial \Delta \alpha}{\partial \Delta \gamma} \right)^2, \end{aligned} \quad (\text{D1})$$

$$\begin{aligned} \frac{\partial^2 \pi_\Delta}{\partial \Delta \gamma \partial \tilde{\mathbf{N}}^s} &= \mathbb{P}_{N^s}^\top : \left(2 \frac{\partial(\psi_e + \tilde{\psi}_k)}{\partial \hat{\mathbf{C}}^p} + 2\Delta \gamma \frac{\partial^2(\psi_e + \tilde{\psi}_k)}{\partial \hat{\mathbf{C}}^{p2}} : 2\mathbf{N}^s \right. \\ &\quad \left. + \sigma_y \frac{\partial^2 \Delta \alpha}{\partial \Delta \gamma \partial \mathbf{N}^s} + 2 \frac{\partial \pi_R}{\partial \hat{\mathbf{C}}^p} + 2\Delta \gamma \frac{\partial^2 \pi_R}{\partial \hat{\mathbf{C}}^{p2}} : 2\mathbf{N}^s \right) \end{aligned}$$

$$+ 2\Delta\gamma \frac{\partial^2 \tilde{\psi}_k}{\partial \hat{\mathbf{C}}^p \partial \hat{\mathbf{C}}^{pd}} : \left(2 \frac{b}{a} \boldsymbol{\Sigma}_n^{b'} \mathbf{C}_n^{pd} \right) + \frac{\partial^2 \psi_n}{\partial \alpha^2} \frac{\partial \Delta \alpha}{\partial \mathbf{N}^s} \frac{\partial \Delta \alpha}{\partial \Delta \gamma}, \quad (\text{D2})$$

$$\begin{aligned} \frac{\partial^2 \pi_\Delta}{\partial \tilde{\mathbf{N}}^{s^2}} &= \mathbb{D}_N^s(\mathbf{A}) + \frac{\partial^2 \pi_R}{\partial \tilde{\mathbf{N}}^{s^2}} \\ &+ \mathbb{P}_{N^s}^\top : \left((2\Delta\gamma)^2 \frac{\partial^2 (\psi_e + \tilde{\psi}_k)}{\partial \hat{\mathbf{C}}^{p^2}} + \frac{\partial^2 \psi_n}{\partial \alpha^2} \frac{\partial \Delta \alpha}{\partial \mathbf{N}^s} \otimes \frac{\partial \Delta \alpha}{\partial \mathbf{N}^s} \right. \\ &\left. + \sigma_y \frac{\partial^2 \Delta \alpha}{\partial \mathbf{N}^{s^2}} + (2\Delta\gamma)^2 \frac{\partial^2 \pi_r}{\partial \hat{\mathbf{C}}^{p^2}} \right) : \mathbb{P}_N^s. \end{aligned} \quad (\text{D3})$$

Here, \mathbb{D}_N^s is defined via

$$d(\mathbb{P}_{N^s}^\top : \mathbf{B}) = \mathbb{D}_N^s(\mathbf{B}) : d\tilde{\mathbf{N}}^s + \mathbb{P}_{N^s}^\top : d\mathbf{B} \quad (\text{D4})$$

and reads

$$\begin{aligned} \mathbb{D}_N^s(\mathbf{B}) &= -\frac{1}{\|\mathbf{U}_n^{p-1} \tilde{\mathbf{N}}^s \mathbf{U}_n^{p-1}\|^3} \left(\mathbf{f}(\mathbf{B}) \otimes \mathbf{C}_n^{p-1} \tilde{\mathbf{N}}^s \mathbf{C}_n^{p-1} \right. \\ &+ \mathbf{C}_n^{p-1} \tilde{\mathbf{N}}^s \mathbf{C}_n^{p-1} \otimes \mathbf{f}(\mathbf{B}) \\ &- \frac{1}{\|\mathbf{U}_n^{p-1} \tilde{\mathbf{N}}^s \mathbf{U}_n^{p-1}\|^2} (\tilde{\mathbf{N}}^s : \mathbf{B}) \mathbf{C}_n^{p-1} \tilde{\mathbf{N}}^s \mathbf{C}_n^{p-1} \otimes \mathbf{C}_n^{p-1} \tilde{\mathbf{N}}^s \mathbf{C}_n^{p-1} \\ &\left. + (\tilde{\mathbf{N}}^s : \mathbf{B}) \mathbf{C}_n^{p-1} \square \mathbf{C}_n^{p-1} \right), \end{aligned} \quad (\text{D5})$$

where \mathbf{B} is an arbitrary second order tensor and $\mathbf{f}(\mathbf{B})$ is defined as

$$\mathbf{f}(\mathbf{B}) = \mathbf{B} - \frac{1}{\|\mathbf{U}_n^{p-1} \tilde{\mathbf{N}}^s \mathbf{U}_n^{p-1}\|^2} (\tilde{\mathbf{N}}^s : \mathbf{B}) \mathbf{C}_n^{p-1} \tilde{\mathbf{N}}^s \mathbf{C}_n^{p-1}. \quad (\text{D6})$$

Likewise, one can define \mathbb{D}_p and \mathbb{D}_{pd} via

$$d(\mathbb{P}_p^\top : \mathbf{B}) = \mathbb{D}_p(\mathbf{B}) : d\hat{\mathbf{C}}^p + \mathbb{P}_p^\top : d\mathbf{B}, \quad (\text{D7})$$

$$\begin{aligned} \Rightarrow \mathbb{D}_p(\mathbf{B}) &= -\frac{1}{3} \hat{\mathbf{M}}^{p-\frac{1}{3}} \left(\left(\mathbf{B} - \frac{1}{3} (\hat{\mathbf{C}}^p : \mathbf{B}) \hat{\mathbf{C}}^{p-1} \right) \otimes \hat{\mathbf{C}}^{p-1} \right. \\ &+ \hat{\mathbf{C}}^{p-1} \otimes \left(\mathbf{B} - \frac{1}{3} (\hat{\mathbf{C}}^p : \mathbf{B}) \hat{\mathbf{C}}^{p-1} \right) \\ &\left. - (\hat{\mathbf{C}}^p : \mathbf{B}) \left(\hat{\mathbf{C}}^{p-1} \square \hat{\mathbf{C}}^{p-1} - \frac{1}{3} \hat{\mathbf{C}}^{p-1} \otimes \hat{\mathbf{C}}^{p-1} \right) \right), \end{aligned} \quad (\text{D8})$$

$$d(\mathbb{P}_{pd}^\top : \mathbf{B}) = \mathbb{D}_{pd}(\mathbf{B}) : d\hat{\mathbf{C}}^{pd} + \mathbb{P}_{pd}^\top : d\mathbf{B}, \quad (\text{D9})$$

$$\Rightarrow \mathbb{D}_{pd}(\mathbf{B}) = \dots \quad (\text{D10})$$

Here, \mathbb{D}_{pd} is worked out in analogy to \mathbb{D}_p , which means just the indexes are changing. The remaining occurring derivatives are given as

$$\frac{\partial^2 (\psi_e + \tilde{\psi}_k)}{\partial \hat{\mathbf{C}}^{p^2}} = \mathbb{D}_p \left(\frac{\partial (\psi_e + \tilde{\psi}_k)}{\partial \mathbf{C}^p} \right) + \mathbb{P}_p^\top : \frac{\partial^2 \psi_e}{\partial \mathbf{C}^{p^2}} : \mathbb{P}_p, \quad (\text{D11})$$

$$\begin{aligned} \frac{\partial^2 \psi_e}{\partial \mathbf{C}^{p^2}} &= \mathbf{C}^{p-1} \mathbf{F}^T \square \mathbf{F} \mathbf{C}^{p-1} : \frac{\partial^2 \psi_e}{\partial \mathbf{b}^{e^2}} : \mathbf{C}^{p-1} \mathbf{F}^T \square \mathbf{F} \mathbf{C}^{p-1} \\ &- \mathbf{C}^{p-1} \square \frac{\partial \psi_e}{\partial \mathbf{C}^p} - \frac{\partial \psi_e}{\partial \mathbf{C}^p} \square \mathbf{C}^{p-1}, \end{aligned} \quad (\text{D12})$$

$$\frac{\partial^2 \tilde{\psi}_k}{\partial \hat{\mathbf{C}}^{pd^2}} = \mathbb{D}_{pd} \left(\frac{\partial \tilde{\psi}_k}{\partial \mathbf{C}^{pd}} \right)$$

$$+ \mathbb{P}_{\text{pd}}^{\text{T}} : \left(\mathbf{C}^{\text{pd}-1} \square^{\text{s}} \frac{\partial \tilde{\psi}_{\text{k}}}{\partial \mathbf{C}^{\text{pd}}} + \frac{\partial \tilde{\psi}_{\text{k}}}{\partial \mathbf{C}^{\text{pd}}} \square^{\text{s}} \mathbf{C}^{\text{pd}-1} \right) : \mathbb{P}_{\text{pd}}, \quad (\text{D13})$$

$$\frac{\partial^2 \tilde{\psi}_{\text{k}}}{\partial \hat{\mathbf{C}}^{\text{p}} \partial \hat{\mathbf{C}}^{\text{pd}}} = -\frac{\mu^{\text{p}}}{2} \mathbb{P}_{\text{p}}^{\text{T}} : \left(\mathbf{C}^{\text{pd}-1} \square^{\text{s}} \mathbf{C}^{\text{pd}-1} \right) : \mathbb{P}_{\text{pd}}, \quad (\text{D14})$$

$$\frac{\partial^2 \pi_{\text{R}}}{\partial \hat{\mathbf{C}}^{\text{p}2} } = \left(\frac{\partial^2 \pi_{\text{R}}}{\partial \hat{\mathbf{m}}^{\text{p}2} } \hat{\mathbf{m}}^{\text{p}} + \frac{\partial \pi_{\text{R}}}{\partial \hat{\mathbf{m}}^{\text{p}} } \right) \hat{\mathbf{m}}^{\text{p}} \hat{\mathbf{C}}^{\text{p}-1} \otimes \hat{\mathbf{C}}^{\text{p}-1} - \frac{\partial \pi_{\text{R}}}{\partial \hat{\mathbf{m}}^{\text{p}} } \hat{\mathbf{m}}^{\text{p}} \hat{\mathbf{C}}^{\text{p}-1} \square^{\text{s}} \hat{\mathbf{C}}^{\text{p}-1}, \quad (\text{D15})$$

$$\frac{\partial^2 \Delta \alpha}{\partial \Delta \gamma^2} = \sqrt{\frac{2}{3}} 2\mathbf{N}^{\text{s}} : \left(\mathbb{D}_{\text{p}} \left(\frac{1}{2} \mathbf{M}_{\text{Cp}} \right) + \mathbb{P}_{\text{p}}^{\text{T}} : \frac{1}{2} \frac{\partial \mathbf{M}_{\text{Cp}}}{\partial \mathbf{C}^{\text{p}}} : \mathbb{P}_{\text{p}} \right) : 2\mathbf{N}^{\text{s}}, \quad (\text{D16})$$

$$\begin{aligned} \frac{\partial^2 \Delta \alpha}{\partial \Delta \gamma \partial \tilde{\mathbf{N}}^{\text{s}}} &= \sqrt{\frac{2}{3}} 2\mathbb{P}_{\text{Ns}}^{\text{T}} : \mathbb{P}_{\text{p}}^{\text{T}} : \frac{1}{2} \mathbf{M}_{\text{Cp}} \\ &+ 2\Delta \gamma \mathbb{P}_{\text{Ns}}^{\text{T}} : \left(\mathbb{D}_{\text{p}} \left(\frac{1}{2} \mathbf{M}_{\text{Cp}} \right) + \mathbb{P}_{\text{p}}^{\text{T}} : \frac{1}{2} \frac{\partial \mathbf{M}_{\text{Cp}}}{\partial \mathbf{C}^{\text{p}}} : \mathbb{P}_{\text{p}} \right) : 2\mathbf{N}^{\text{s}}, \end{aligned} \quad (\text{D17})$$

$$\begin{aligned} \frac{\partial^2 \Delta \alpha}{\partial \tilde{\mathbf{N}}^{\text{s}2}} &= \sqrt{\frac{2}{3}} 2\Delta \gamma \mathbb{D}_{\text{N}}^{\text{s}} \left(\mathbb{P}_{\text{p}}^{\text{T}} : \frac{1}{2} \mathbf{M}_{\text{Cp}} \right) \\ &+ (2\Delta \gamma)^2 \mathbb{P}_{\text{Ns}}^{\text{T}} : \left(\mathbb{D}_{\text{p}} \left(\frac{1}{2} \mathbf{M}_{\text{Cp}} \right) + \mathbb{P}_{\text{p}}^{\text{T}} : \frac{1}{2} \frac{\partial \mathbf{M}_{\text{Cp}}}{\partial \mathbf{C}^{\text{p}}} : \mathbb{P}_{\text{p}} \right) \mathbb{P}_{\text{N}}^{\text{s}}, \end{aligned} \quad (\text{D18})$$

$$\begin{aligned} \frac{\partial^2 \pi_{\text{R}}}{\partial \tilde{\mathbf{N}}^{\text{s}2}} &= A \left(\mathbf{C}_{\text{n}}^{\text{p}-1} \square^{\text{s}} \mathbf{C}_{\text{n}}^{\text{p}-1} \left(1 - \frac{1}{\| \mathbf{U}_{\text{n}}^{\text{p}-1} \tilde{\mathbf{N}}^{\text{s}} \mathbf{U}_{\text{n}}^{\text{p}-1} \|} \right) \right. \\ &\left. + \frac{1}{\| \mathbf{U}_{\text{n}}^{\text{p}-1} \tilde{\mathbf{N}}^{\text{s}} \mathbf{U}_{\text{n}}^{\text{p}-1} \|} \mathbf{C}_{\text{n}}^{\text{p}-1} \mathbf{N}^{\text{s}} \mathbf{C}_{\text{n}}^{\text{p}-1} \otimes \mathbf{C}_{\text{n}}^{\text{p}-1} \mathbf{N}^{\text{s}} \mathbf{C}_{\text{n}}^{\text{p}-1} \right), \end{aligned} \quad (\text{D19})$$

$$\begin{aligned} \frac{\partial \mathbf{M}_{\text{Cp}}}{\partial \mathbf{C}^{\text{p}}} &= \frac{1}{\| \mathbf{U}_{\text{n}}^{\text{p}-1} \Delta \mathbf{C}^{\text{p}} \mathbf{U}_{\text{n}}^{\text{p}-1} \|} \left(\mathbf{C}_{\text{n}}^{\text{p}-1} \square^{\text{s}} \mathbf{C}_{\text{n}}^{\text{p}-1} - \mathbf{M}_{\text{Cp}} \otimes \mathbf{M}_{\text{Cp}} \right) \\ &+ a_2 \left(\mathbf{C}_{\text{n}}^{\text{p}-1} \otimes \mathbf{C}_{\text{n}}^{\text{p}-1} - \mathbf{C}_{\text{n}}^{\text{p}-1} \square^{\text{s}} \mathbf{C}_{\text{n}}^{\text{p}-1} \right). \end{aligned} \quad (\text{D20})$$

APPENDIX E. CONSISTENT TANGENT

When solving boundary value problems using the finite element method, we make use of the consistent tangent operator $\underline{\mathbb{C}}^{\text{algo}}$. This is derived in this model as follows. We start with the virtual work of the internal forces

$$\int_{V_0} \boldsymbol{\tau} : \mathbf{d}_{\delta} dV, \quad (\text{E1})$$

where \mathbf{d}_{δ} is defined as

$$\mathbf{d}_{\delta} = \text{sym} \underbrace{\left(\text{Grad}(\delta \mathbf{u}) \mathbf{F}^{-1} \right)}_{\mathbf{l}_{\delta}}. \quad (\text{E2})$$

Now, calculating the differential, we get

$$\int_{V_0} d(\boldsymbol{\tau} : \mathbf{d}_{\delta}) dV. \quad (\text{E3})$$

Further, expressing the differential in terms of \mathbf{S} and \mathbf{F} , we get

$$d(\boldsymbol{\tau} : \mathbf{d}_{\delta}) = d(\boldsymbol{\tau} : \mathbf{l}_{\delta}) = d(\mathbf{F}\mathbf{S}) : \delta \mathbf{F}, \quad (\text{E4})$$

where the symmetry of τ was exploited. Now, the differential is calculated to be

$$\begin{aligned} d(\mathbf{FS}) : \delta \mathbf{F} &= (d\mathbf{FS}) : \delta \mathbf{F} \\ &= (d\mathbf{FF}^{-1}\mathbf{FSF}^T(\delta\mathbf{FF}^{-1})^T) : \mathbf{I} + (\mathbf{FdSF}^T) : \mathbf{l}_\delta \\ &= (\mathbf{l}_d\tau\mathbf{l}_\delta) : \mathbf{I} + (\mathbb{C}^{\text{algo}} : \mathbf{d}_d) : \mathbf{l}_\delta. \end{aligned} \quad (\text{E5})$$

Here, the first term is the so-called geometric tangent and the second term arises from the elastic and inelastic contributions to the materials stiffness. Additionally, \mathbf{l}_d and \mathbf{d}_d are defined in analogy to \mathbf{l}_δ and \mathbf{d}_δ . Further, $\mathbb{C}^{\text{algo}} : \mathbf{d}_d$ can be split into the elastic and inelastic part:

$$\begin{aligned} \mathbb{C}^{\text{algo}} : \mathbf{d}_d &= \left(\mathbf{F} \square \mathbf{F}^T : \frac{\partial \mathbf{S}}{\partial \mathbf{E}} : \mathbf{F}^T \square \mathbf{F} \right) : \mathbf{d}_d + \frac{\partial(\mathbf{FSF}^T)}{\partial \mathbf{z}} : \frac{\partial \mathbf{z}}{\partial \mathbf{E}} : d\mathbf{E} \\ &= \mathbb{C}^{\text{algo,e}} : \mathbf{d}_d + \frac{\partial \tau}{\partial \mathbf{z}} \frac{\partial \mathbf{z}}{\partial \mathbf{E}} : \mathbf{F}^T \mathbf{d}_d \mathbf{F}. \end{aligned} \quad (\text{E6})$$

Now, to evaluate $\partial \mathbf{z} / \partial \mathbf{E}$, we have a look at the local newton scheme, where

$$\frac{\partial \pi_\Delta}{\partial \mathbf{z}} = 0 \quad (\text{E7})$$

must hold in the converged state. Therefore, calculating the differential of Equation (E7), we obtain

$$\begin{aligned} 0 &= d\left(\frac{\partial \pi_\Delta}{\partial \mathbf{z}}\right) \\ &= \frac{\partial^2 \pi_\Delta}{\partial \mathbf{z}^2} d\mathbf{z} + \frac{\partial^2 \pi_\Delta}{\partial \mathbf{z} \partial \mathbf{E}} : d\mathbf{E} = 0 \\ &= \frac{\partial^2 \pi_\Delta}{\partial \mathbf{z}^2} d\mathbf{z} + \left(\frac{\partial \mathbf{S}}{\partial \mathbf{z}}\right)^T : d\mathbf{E} = 0. \end{aligned} \quad (\text{E8})$$

Now, rearranging Equation (E8), we get

$$\begin{aligned} d\mathbf{z} &= -\left(\frac{\partial^2 \pi_\Delta}{\partial \mathbf{z}^2}\right)^{-1} \frac{\partial^2 \pi_\Delta}{\partial \mathbf{z} \partial \mathbf{E}} : d\mathbf{E} \\ &= -\frac{\partial \mathbf{z}}{\partial \mathbf{E}} : d\mathbf{E} \\ &= -\left(\frac{\partial^2 \pi_\Delta}{\partial \mathbf{z}^2}\right)^{-1} \left(\frac{\partial \mathbf{S}}{\partial \mathbf{z}}\right)^T : \mathbf{F}^T \square \mathbf{F} : \mathbf{d}_d \\ &= -\left(\frac{\partial^2 \pi_\Delta}{\partial \mathbf{z}^2}\right)^{-1} \left(\frac{\partial \tau}{\partial \mathbf{z}}\right)^T : \mathbf{d}_d. \end{aligned} \quad (\text{E9})$$

Inserting the relation for $\partial \mathbf{z} / \partial \mathbf{E}$ into Equation (E6), we finally obtain the algorithmic tangent:

$$\mathbb{C}^{\text{algo}} = \mathbb{C}^{\text{algo,e}} - \frac{\partial \tau}{\partial \mathbf{z}} \left(\frac{\partial^2 \pi_\Delta}{\partial \mathbf{z}^2}\right)^{-1} \left(\frac{\partial \tau}{\partial \mathbf{z}}\right)^T. \quad (\text{E10})$$

Here, the term $\partial \tau / \partial \mathbf{z}$ is calculated via

$$\frac{\partial \tau}{\partial \mathbf{z}} = \begin{pmatrix} \frac{\partial \tau}{\partial \Delta \gamma} \\ \frac{\partial \tau}{\partial \hat{\mathbf{N}}^s} \end{pmatrix}, \quad (\text{E11})$$

where the occurring derivatives of τ are given by

$$\frac{\partial \tau}{\partial \Delta \gamma} = 2 \frac{\partial \tau}{\partial \hat{\mathbf{C}}^p} : \mathbf{N}^s, \quad (\text{E12})$$

$$\frac{\partial \boldsymbol{\tau}}{\partial \tilde{\mathbf{N}}^s} = 2\Delta\gamma \frac{\partial \boldsymbol{\tau}}{\partial \hat{\mathbf{C}}^p} : \mathbb{P}_{N^s}^\top, \quad (\text{E13})$$

$$\begin{aligned} \frac{\partial \boldsymbol{\tau}}{\partial \hat{\mathbf{C}}^p} &= -2 \left(\mathbf{I}^s \frac{\partial \psi_e}{\partial \mathbf{b}^e} + \frac{\partial \psi_e}{\partial \mathbf{b}^e} \mathbf{I}^s + \left(\mathbf{I}^s \mathbf{b}^e + \mathbf{b}^e \mathbf{I}^s \right) : \frac{\partial^2 \psi_e}{\partial \mathbf{b}^{e2}} \right) \\ &: \mathbf{F}^s \mathbf{F}^{T^s} : \mathbf{C}^{p-1} \mathbf{C}^{p-1} : \mathbb{P}_p. \end{aligned} \quad (\text{E14})$$